NEOPLASIA
www.neoplasia.com

Volume 12 Number 6 June 2010 pp. 453–463 453

Invasive Glioblastoma Cells Acquire Stemness and Increased Akt Activation[1,2]

Jennifer R. Molina*, Yuho Hayashi*, Clifton Stephens† and Maria-Magdalena Georgescu*

*Department of Neuro-oncology, The University of Texas MD Anderson Cancer Center, Houston, TX, USA;
†Department of Veterinary Medicine and Surgery, The University of Texas MD Anderson Cancer Center, Houston, TX, USA

Abstract

Glioblastoma multiforme (GBM) is the most frequent and most aggressive brain tumor in adults. The dismal prognosis is due to postsurgery recurrences arising from escaped invasive tumor cells. The signaling pathways activated in invasive cells are under investigation, and models are currently designed in search for therapeutic targets. We developed here an *in vivo* model of human invasive GBM in mouse brain from a GBM cell line with moderate tumorigenicity that allowed simultaneous primary tumor growth and dispersal of tumor cells in the brain parenchyma. This strategy allowed for the first time the isolation and characterization of matched sets of tumor mass (Core) and invasive (Inv) cells. Both cell populations, but more markedly Inv cells, acquired stem cell markers, neurosphere renewal ability, and resistance to rapamycin-induced apoptosis relative to parental cells. The comparative phenotypic analysis between Inv and Core cells showed significantly increased tumorigenicity *in vivo* and increased invasion with decreased proliferation *in vitro* for Inv cells. Examination of a large array of signaling pathways revealed extracellular signal–regulated kinase (Erk) down-modulation and Akt activation in Inv cells and an opposite profile in Core cells. Akt activation correlated with the increased tumorigenicity, stemness, and invasiveness, whereas Erk activation correlated with the proliferation of the cells. These results underscore complementary roles of the Erk and Akt pathways for GBM proliferation and dispersal and raise important implications for a concurrent inhibitory therapy.

Neoplasia (2010) 12, 453–463

Introduction

Glioblastoma multiforme (GBM) is the most aggressive form of gliomas, accounting for approximately 50% of all glial tumor types. GBMs are astrocytic-type tumors that may arise *de novo* in more than 90% of cases or secondary to the progression of lower-grade astrocytomas in less than 10% of cases [1]. GBMs are refractory to conventional treatment approaches and have a median survival in the range of 12 to 15 months. Three features of this tumor make it resistant to therapy: the presence of the blood-brain barrier that restricts drug distribution to the brain, the heterogeneity of the tumor that consists of cell populations with different drug sensitivities, and the propensity of the tumor cells to infiltrate the normal brain leading to recurrences [2]. Overall, the dismal prognosis of GBM patients is attributable to drug-resistant relapsing foci arising from infiltrating tumor cells spreading at a distance from the primary tumor core.

The most frequent genetic alteration in primary GBM is the 10q chromosome deletion in 70% of cases, followed by alterations that either deregulate the cell cycle by targeting the Rb and p53 pathways or boost cell growth by epidermal growth factor receptor (EGFR) amplification, overexpression or expression of a constitutively active mutant form [1,3]. EGFR signaling results in the downstream activation of the extracellular signal–regulated kinase (Erk) and phosphatidylinositol

Abbreviations: GBM, glioblastoma multiforme; Erk, extracellular signal–regulated kinase; PI3K, phosphatidylinositol 3-OH kinase; ECM, extracellular matrix; GFP, green fluorescent protein; PHLPP, PH domain leucine-rich repeat protein phosphatase

Address all correspondence to: Maria-Magdalena Georgescu, MD, PhD, MD Anderson Cancer Center, Unit 1002, 6767 Bertner Ave, Houston, TX 77030.
E-mail: mgeorges@mdanderson.org

[1]This work was supported by National Cancer Institute grant CA107201 and MD Anderson Cancer Center institutional research grant to M.-M.G.
[2]This article refers to supplementary materials, which are designated by Figures W1 to W4 and are available online at www.neoplasia.com.
Received 8 January 2010; Revised 16 March 2010; Accepted 18 March 2010

DOI 10.1593/neo.10126

3-OH kinase (PI3K)/Akt pathways. An extra layer of activation of these pathways in GBM occurs through the inactivation of the upstream tumor suppressors of the pathways, NF1 and PTEN, respectively [3,4].

Signaling through both Erk and PI3K/Akt has been implicated in facilitating the GBM cell invasion triggered by cell attachment to extracellular matrix (ECM) [5]. However, the pathways that lead to enhanced invasiveness of GBM cells are not well characterized. It is important to bear in mind not only that it is the interaction between the GBM cells and the brain ECM microenvironment that triggers the invasion of the GBM cells but also that GBM cells secrete ECM components that could also modify their migration [6,7].

To uncover what pathways are important for the accelerated dispersal of the GBM cells into the brain parenchyma, we developed a model of human invasive GBM cells in the brain parenchyma of immunodeficient mice. Isolation and characterization of sets of matched tumor core cells and invasive cells slowly growing out within the brain from the same pool of parental cells revealed acquisition of stem cell properties and complementary proliferation and invasive phenotypes of the cell populations. Further analysis uncovered a cross talk between the PI3K and Erk pathways in GBM cells that underlies the observed phenotypes.

Materials and Methods

Vectors, Transfections, and Infections

293T cells, U251-MG GBM cells, and normal human astrocytes (NHAs; gift from T.J. Liu) were grown in Dulbecco's modified Eagle medium (DMEM) supplemented with 10% FBS. The complementary DNA for the enhanced green fluorescent protein (GFP) was inserted in the pCX_p retroviral vector (puromycin selection), and the complementary DNA for mCherry (gift from Roger Y. Tsien) was inserted in the pCX_b vector (blasticidin selection). Transfections and retroviral infections were performed as described [8]. U251-MG and NHAs were infected with GFP- or mCherry-containing retroviruses, respectively, and subjected to 14 days of drug selection to stably express the markers.

Orthotopic Intracranial Injections

For intracranial cell implantation of U251-GFP–labeled parental cells into the right hemisphere at a point situated 2.5 mm anterior and lateral from the bregma, the implantable guide-screw system was used on 6-week-old severe combined immunodeficient (SCID) mice (Jackson Laboratory, Bar Harbor, ME) [9]. A total of 2×10^6 GFP-labeled U251-MG cells were washed and resuspended in 15 μl of DMEM containing 0.7 μg/ml Matrigel (BD Biosciences, San Jose, CA). The mice were anesthetized, and the cell suspension was slowly injected into the bolt using a Hamilton syringe attached to the PDH 2000 Infusion machine (Harvard Apparatus, Holliston, MA). The wound was clipped closed, sterilized with Betadine (Purdue Pharma, Stanford, CT), and mice were followed up for brain tumor development. Injections for the tumor mass (Core) and invasive (Inv) cells were performed similarly by direct intracranial injection of 2×10^6 cells.

Establishment of the Core and Inv Cell Lines

Once the mice developed strong neurological symptoms because of brain tumor burden, they were killed in a CO_2 chamber, and the brains were immediately collected and were either fixed in formalin for pathological analysis or placed into a sterile dish containing PBS for further dissection and cell collection. Images of the whole brain with U251-GFP cells *in situ* were obtained with a fluorescence Zeiss Axiovert 200M microscope (Carl Zeiss MicroImaging, Thronwood, NY) before cell collection. The right frontal lobe containing the injection site and the tumor core was dissected from the rest of the brain containing the invasive tumor cells. Both brain sections were separately triturated with a scalpel, pelleted, resuspended in 0.25% trypsin-EDTA, and rotated on a warm plate for 15 minutes. Cells were centrifuged and resuspended in DMEM, 10% FBS, and 0.5 μg/ml puromycin to ensure purity of the culture. The Inv and Core cells were isolated and constantly grown on Matrigel (0.7 mg/ml)-coated dishes. In these conditions, they maintained their differential proliferation phenotype for at least 6 to 10 passages in culture. Freshly isolated cells were expanded in culture for two passages taking approximately 2 weeks, before early frozen stocks were prepared. For mouse reinjection, fresh cells at passage 2 were used. For the other experiments, including proliferation, invasion, neurosphere formation, and Western blot analysis, cells derived from the early stocks after one or two additional passages were used.

Histology and Immunostaining

Brains were embedded in paraffin, and 4-μm sections were processed for hematoxylin and eosin (H&E) staining or immunohistochemistry (IHC) as previously described [10,11]. For IHC, the primary antibodies GFP, phospho-Erk (P-Erk), and phospho-Akt (S473) were used at 1:300 dilution (see also below for antibody information). Immunofluorescence analysis was performed as described [12]. Image stacks were acquired with a Zeiss Axiovert 200M inverted microscope and deconvolved with the AxioVision Rel 4.5 SP1 software (Carl Zeiss MicroImaging).

Invasion Assays

To assess cell invasiveness, a new three-dimensional invasion assay was used, which uses a method for levitated cell culturing where cells grown in monolayer cultures at 80% confluence are treated with 1 μl of hydrogel per 1 cm^2 of surface area [13,14]. As a representation of the normal brain parenchyma, we used NHAs stably expressing mCherry. NHA-mCherry and Inv-GFP or Core-GFP cells pretreated with hydrogel were detached by treating with trypsin-EDTA and placed into a new tissue culture Petri dish containing DMEM–10% FBS. A top with an attached neodymium magnet covered the dish to induce levitation and formation of three-dimensional spheres of gel-treated cells in 3 to 5 days. Once structures of similar sizes were achieved, an NHA-mCherry sphere was placed in the same dish with either an Inv-GFP or Core-GFP sphere, while the neodymium magnet on the cover brought structures together. The subsequent infiltration of the GBM-GFP cells among the NHA-mCherry cells was recorded with a Zeiss Axiovert 200M inverted microscope, and images were deconvolved with the AxioVision Rel 4.5 SP1 software. For the Matrigel invasion assay, 1×10^6 cells were prepared in duplicate in 250 μl of serum-free DMEM. The cells were placed in transwells with 8-μm pore size polycarbonate filters (Corning Incorporated, Corning, NY), precoated with 100 μl of 0.7 mg/ml Matrigel (BD Biosciences). The lower wells were filled with 750 μl of DMEM. The cells were incubated at 37°C for 24 hours, fixed with methanol, and stained with H&E. Nonmigratory cells on the upper surface of the transwells were removed with a cotton swab, and the migratory cells from the lower surface of the

transwell were solubilized in 500 μl of 2% (wt./vol.) sodium dodecyl sulfate solution. The intensity of the dye was quantified by measuring the absorbance at 620 nm with a Beckman spectrophotometer DU640 (Beckman Coulter, Brea, CA).

Proliferation and Apoptosis

The 3-(4,5-dimethylthiazol-2-yl)-2,5-diphenyltetrazolium bromide (MTT; Sigma-Aldrich, St Louis, MO) assay was used to measure proliferation, as described [15]. For the apoptosis assay, 5000 cells were plated on eight-chamber slides and allowed to attach overnight. Once attached, cells were treated with rapamycin (100 nM/ml) for 72 hours. Apoptosis detection was performed with the *In Situ* Cell Death Detection Kit, TMR Red (New England Biolabs, Ipswich, MA), as specified by the manufacturer (Figure W2).

Neurosphere Formation and Renewal Assays

A total of 10^4 U251-MG parental, Inv, and Core cells were seeded in triplicates in 60-mm low-binding dishes containing 6 ml of neurosphere growth medium (DMEM F12, B27, 20 ng/ml epidermal growth factor, and 20 ng/ml basic fibroblast growth factor) and were allowed to grow for 2 weeks/passage. The growth factors were replenished every 7 days. For the renewal assay, six individual neurospheres of similar sizes were separated into microcentrifuge tubes, washed once with PBS, incubated in 0.25% trypsin-EDTA for 10 minutes at 37°C, and then homogenized and returned to the neurosphere growth medium. For quantification, 10 aliquots of 100 μl each were taken from each neurosphere dish and plated separately into 10 wells of a 96-well plate. Bright field images of each well were acquired, and the average number of neurospheres was calculated. The average neurosphere area size was measured with the ImageJ software (NIH, Bethesda, MD).

Protein Analysis and Antibodies

The protocols for cell lysis and Western blot analysis were previously described [12]. Antibodies used include the following: Erk1 (C-16, rabbit polyclonal), Erk2 (C-14, rabbit polyclonal), and glyceraldehyde 3-phosphate dehydrogenase (sc-47724, mouse monoclonal) from Santa Cruz Biotechnology (Santa Cruz, CA); phospho-Ser473-Akt (rabbit polyclonal), Akt/protein kinase B (rabbit polyclonal), and phospho-p44-p42-T202/Y204-MAP kinase (P-Erk, mouse monoclonal) from Cell Signaling (Danvers, MA); PH domain leucine-rich repeat protein phosphatases 1 and 2 (PHLPP1 and PHLPP2; rabbit polyclonal) from Bethyl Laboratories (Montgomery, TX); CD133 (rabbit polyclonal) from Abcam (Cambridge, MA); β-tubulin (mouse monoclonal) from Sigma; and GFP (mouse monoclonal), nestin (mouse monoclonal), glial fibrillary acidic protein (GFAP; rabbit polyclonal), and actin (mouse monoclonal) from Chemicon/Millipore (Billerica, MA).

Results

In Vivo Selected Human GBM Cells Induce Invasive Tumors in SCID Mice Resembling Human Disease

Human GBM cells lines have been widely used in mouse xenograft models, especially the highly tumorigenic but noninvasive cell line U87-MG [16]. In this study, we tested the tumorigenicity in immunodeficient animals of an array of GBM cell lines (not shown), and we used the weakly tumorigenic cell line U251-MG to analyze the molecular mechanisms of *in vivo* tumor dispersal. For tracking, parental cells were engineered to stably express GFP, this did not change the phenotypic characteristics of the cells (Figure W1). The moderate tumorigenicity of our stock of U251-MG cells proved optimal for this study because longer mouse survival allowed time for infiltration of the brain with invasive cells (Figure 1). SCID mice intracranially injected with U251-GFP–labeled cells demonstrated a biphasic survival pattern extending for 40 weeks (Figure 1*A*). Surprisingly, two distinct histopathological variants were observed in tumors isolated from these mice. With one exception, mice succumbing earlier than 20 weeks after inoculation developed tumors with parental-like cell morphology. The longer-time survivors developed well-circumscribed heterogeneous tumors with multinucleated giant cells (Figure 1, *A* and *B*). The cells isolated from the tumor of the longest surviving animal (Figure 1*A*) maintained giant morphology and grew poorly in culture (Figure W2), correlating the culture findings with the slow growth rate of these tumors in mice.

To isolate the cells that infiltrated the brain, the brain quadrant containing the primary tumor developing at the injection site was dissected from the rest of the brain (Figure 1*C*). In the dissected material, foci of GFP-labeled tumor cells were visualized at the injection site and in the opposite hemisphere, and paired cultures of GFP-expressing cells were obtained from each dissected brain (Figure 1*D*). Cells isolated from the primary tumor were labeled as Core, and invasive cells isolated from the remaining three quadrants were labeled as Inv.

To analyze the tumorigenic characteristics of the Core and Inv cells, three distinct pairs of cells obtained from the first three short-term surviving mice (Figure 1*A*) were reinjected into SCID mice. Surprisingly, Inv cells uniformly killed the animals twice as fast as Core cells (Figure 2*A*). Paraffin sections were prepared from dissected brains and examined for tumor cell infiltration. The Core cells formed large bulky tumors that detached in some places from the brain on sectioning (Figure 2, *B* and *C*, *arrow*). In contrast, the Inv cells did not grow as bulky tumors but massively infiltrated the ependyma, neuropil, and meninges, including the space between the caudal cerebrum and the cerebellum (Figure 2*B*, *arrows*). Marked dilatation of all ventricles was observed in mice inoculated with Inv cells, most likely accounting for the accelerated course of the neurological disease in these animals. The Core cells also appeared to invade in ball-like structures in the proximity of the main tumor mass, but Inv cells traveled at long distances in small clusters encircling blood vessels, a phenomenon known as satellitosis (Figure 2*C*).

To characterize the patterns of migration and confirm the identity of the Inv infiltrating cells, we performed immunostaining with GFP antibody that labels GFP-expressing tumor cells. Several patterns of migration encountered in human GBM [17,18] were identified in mice inoculated with Inv cells (Figure 2*D*), indicating similitude between this mouse model and human GBM.

In Vitro Testing of In Vivo–Selected Invasive GBM Cells Reveal Increased Invasion and Decreased Proliferation

The invasive capacity of the Inv and Core cells was tested *in vitro* in a new three-dimensional invasion assay on the basis of magnetic levitation that allows infiltration of NHAs by GBM cells (Figure 3*A*) [13]. Individual three-dimensional structures of Inv-GFP and Core-GFP cells were brought in contact with NHA-mCherry by the magnetic field (Figure 3*B*). After contact was established, the three-dimensional assemblies were imaged at different time points (Figure 3*C*). Whereas the edge of the Core cell spheres remained intact and only very few cells escaped and invaded into the astrocyte structure (Figure 3*C*, *right panel*, *dotted contour* and *arrows*), the edge of Inv cell spheres breached,

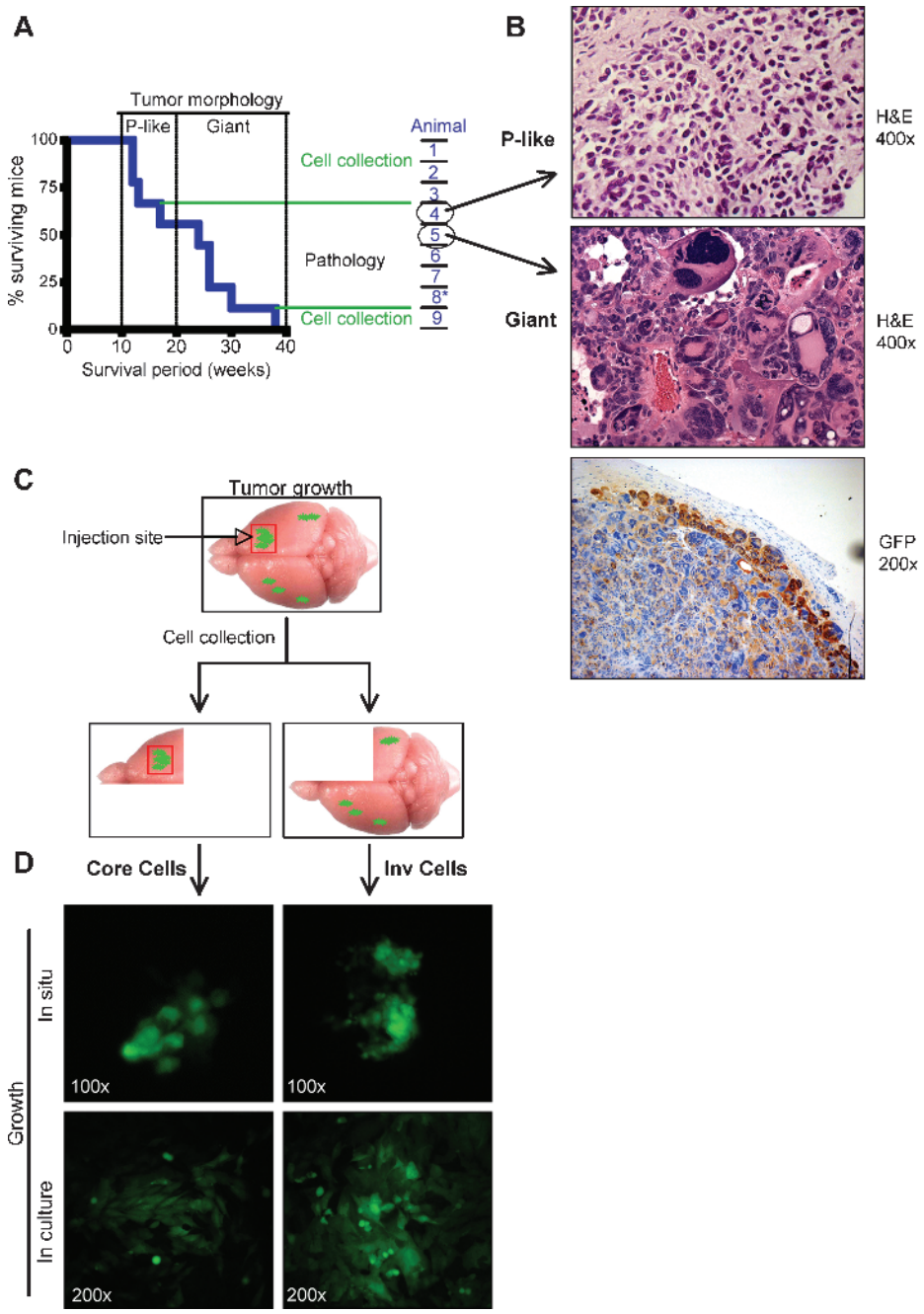

Figure 1. Isolation of invasive (Inv) GBM cells *in vivo*. (A) Kaplan-Meier survival curve of SCID mice ($n = 9$) inoculated intracranially with GFP-labeled parental U251-MG cells. The biphasic mouse survival pattern segregates tumor morphology into parental (P)-like (survival < 20 weeks) or giant cell (survival > 20 weeks) except for animal 8* that developed P-like tumor. On the right, the processing route of the isolated brains is indicated. (B) H&E staining showing the two tumor morphologies identified from the animals circled in (A). The IHC with anti-GFP antibody confirms the U251 origin of the giant multinucleated cells. (C) Procedure scheme: the upper panel depicts a mouse brain and the site of injection of GFP-labeled parental cells (red square). The right front quadrant containing the core of the tumor (right panel) and the remaining three quadrants containing invasive cells (left panel) were processed separately for isolation of pairs of Core and Inv cells, respectively. (D) Fluorescent visualization of the two GFP-labeled cell populations growing *in situ*, in the brain of mice (upper panels), and after isolation in culture (lower panels).

and most peripheral cells extensively penetrated between the NHAs (Figure 3*C*, *left panel*, *dotted contour*). A conventional Matrigel invasion transwell assay was also performed with these cells and showed a small enhancement of the invasive ability of Inv cells compared with Core or parental cells (Figure 3*D*). Taken together, these experiments show that Inv cells demonstrated enhanced invasiveness *in vitro*, both by infiltrating NHA cells, as shown in the three-dimensional magnetic levitation assay, and by invading the ECM, as shown in the Matrigel assay.

In contrast to the increased invasiveness, the proliferation rate of Inv cells was significantly reduced compared with Core cells (Figure 3*E*). U251 parental cells had an intermediate proliferation rate. Altogether, these experiments showed increased invasiveness and decreased proliferation for Inv cells *versus* Core cells.

In Vivo–Selected Invasive GBM Cells Acquire Stem Cells Characteristics

When comparing Inv to Core cells, it becomes apparent that the *in vitro* proliferation phenotype did not correlate with the *in vivo* tumorigenesis. Another possibility for Inv cells to be more tumorigenic would be that a higher number of cells within the population have stem cell properties inducing more tumor foci in mice. We first analyzed the expression of nestin and CD133, as markers for neural stem cells, and of GFAP, as a marker of astrocytic differentiation. Nestin was upregulated in Inv cells compared with both parental and Core cells, and GFAP was upregulated in Core cells (Figure 4, *A* and *B*). CD133 was upregulated in both *in vivo*–derived populations compared with parental cells (Figure 4*B*), suggesting that, although both populations acquired stem cell markers, Inv cells appeared less differentiated than Core cells.

A property of stem cells is the long-term self-renewal or "stemness." Tumor stem cells derived from GBM can form and be propagated as neurospheres when grown in suspension [19]. When we analyzed the neurosphere-forming ability at the first passage of suspended cells, equal numbers of neurospheres resulted from parental, Inv, or Core cells (Figure 4*C*, *upper row*). Core cells formed much larger neurospheres, compared with the others, most likely because of their enhanced proliferation rate. When we propagated the cells for neurosphere renewal, Inv cells formed a higher number of neurospheres than Core cells, whereas parental cells were unable to renew neurospheres at all (Figure 4*C*, *lower row*). Renewal Core neurospheres

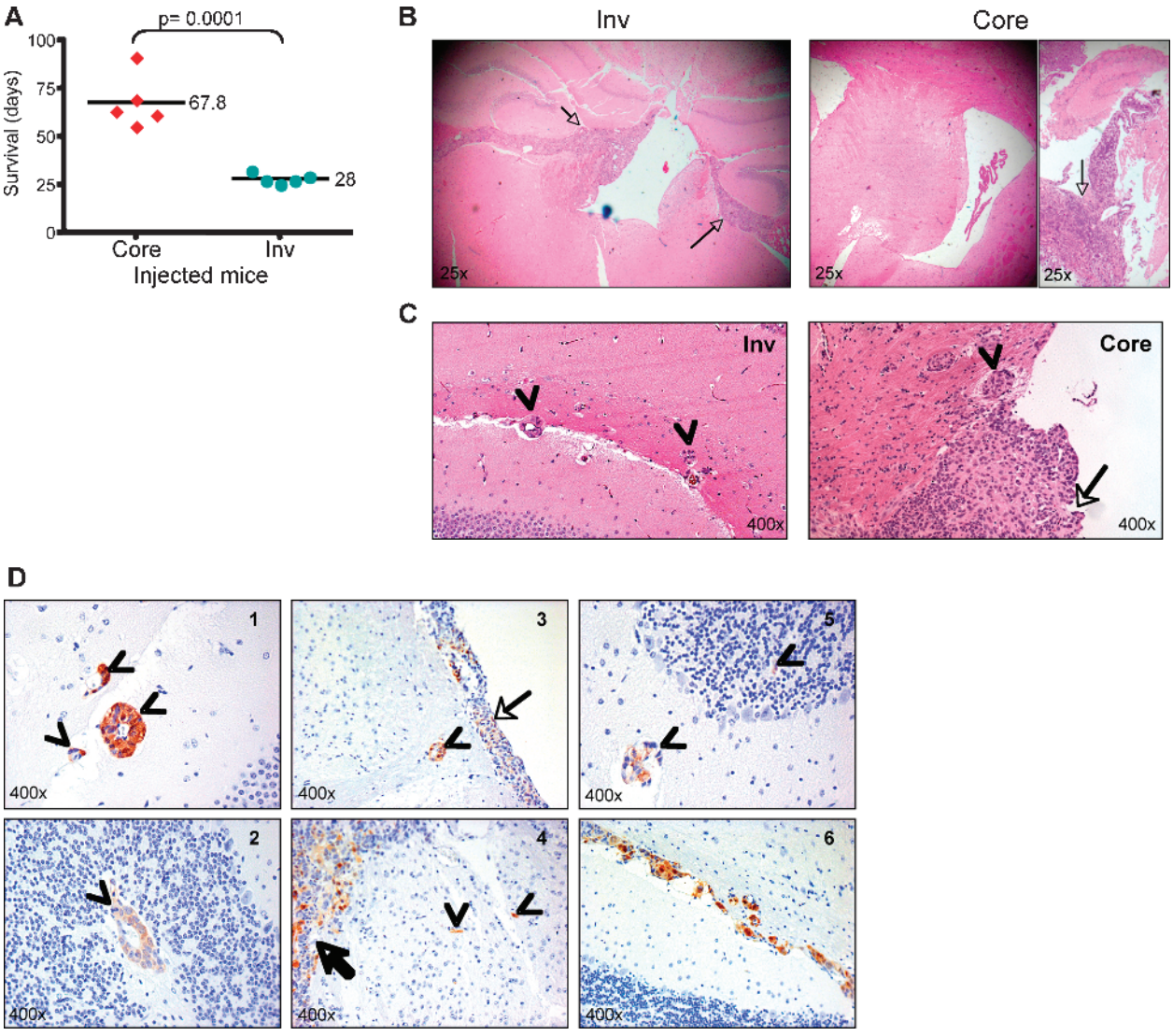

Figure 2. Inv cells are more tumorigenic *in vivo* than Core cells. (A) Survival of mice inoculated with the three pairs of Core and Inv cells isolated from the brains of the mice 1, 2, and 3 shown in Figure 1*A*. Survival periods are expressed as individual values distributed around the mean. (B) H&E showing gross morphology of the brain (original magnification, ×25). Note infiltration with Inv cells of ependyma and meninges (arrows) with marked dilatation of the third ventricle. Note also bulky detached tumors (arrow) of Core cells without infiltration of the ventricles (left panel). (C) H&E showing infiltration of the brain parenchyma by cells detached from the main tumor mass in mice inoculated with either Core or Inv cells. Arrows indicate the main tumor mass; arrowheads, the infiltrative cells. (D) Patterns of migration of Inv cells in the brain of mice. IHC with GFP antibody distinguishes the tumor cells from the normal parenchyma. Arrows indicate the tumor mass; arrowheads, infiltrative cells. Note several patterns of migration: in clusters surrounding blood vessels (satellitosis), in the white matter (1 and 5), the gray matter (2), or in the white matter tracts (3); migration as separate cells (4 and 5); and migration as trains of cells along the white matter tracts (6).

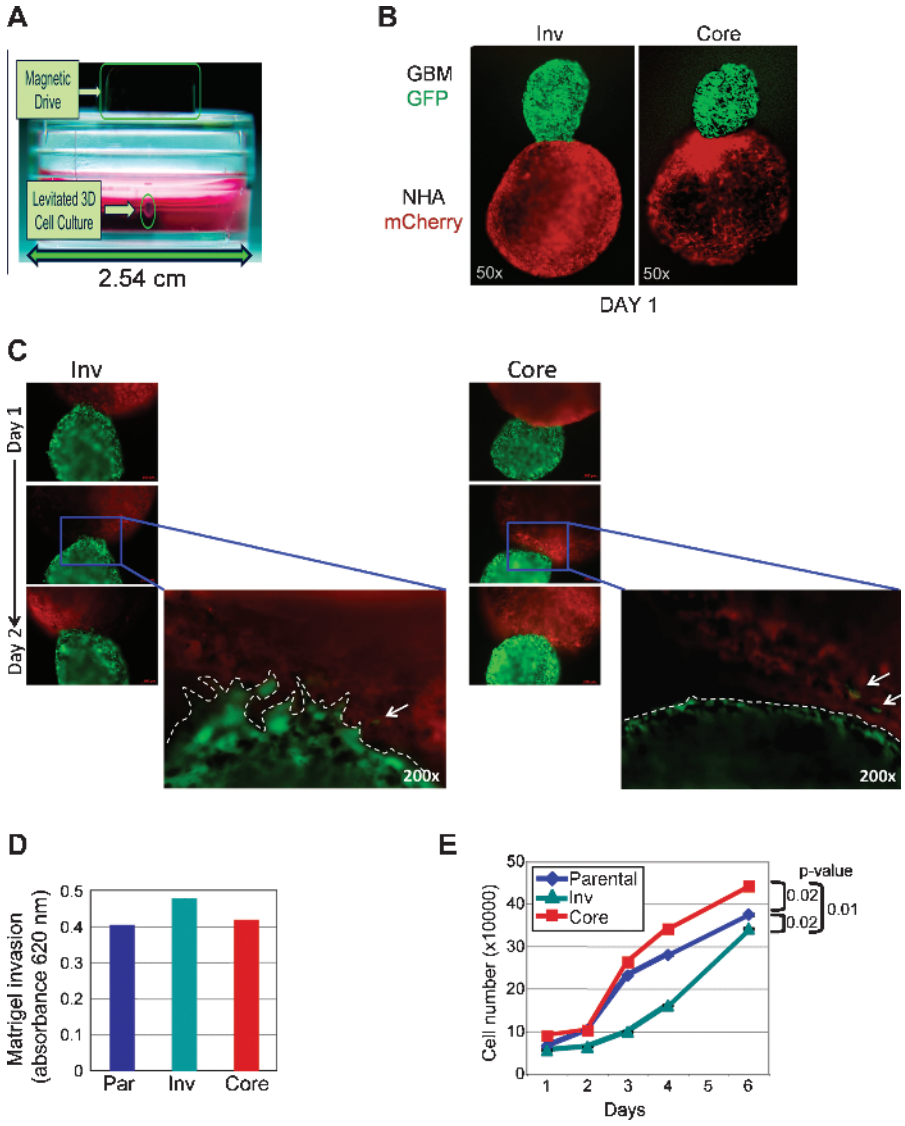

Figure 3. *In vivo*–selected Inv cells demonstrate increased invasion and decreased proliferation relative to Core cells. (A) Three-dimensional *in vitro* invasion assay setup: the GBM or NHA cells treated with Au-Phage-FeO (Levitated 3D Cell Culture) were held in suspension by the magnetic field of a magnet attached to the top of the tissue culture plate (Magnetic Drive). (B) Three-dimensional spheres were allowed to form separately from GFP-labeled Inv and Core cells and from mCherry-labeled NHAs and magnetically guided together. (C) Serial fluorescence images for 48 hours of GBM-NHA composites show an invading front of Inv cells at the contact area with NHAs (dotted line) in contrast to the unaltered surface maintained by Core cells in contact with NHAs. (D) Matrigel invasion assay showing increased invasion of Inv cells compared with parental (Par) or Core cells. (E) MTT proliferation assay of U251-MG parental, Inv, and Core cells shows higher proliferation of Core cells. Data are means ± SEM from triplicates. *P* values were computed by using paired *t* test. These experiments were repeated three times with similar results.

were still larger than Inv neurospheres, although the size difference dropped from 2.5-fold for the first passage to 1.6-fold for renewal neurospheres (Figure 4*C*, *graphs*). As for the cultured cells, renewal Inv neurospheres showed a higher expression of nestin, whereas Core neurospheres showed a higher expression of GFAP that was mainly distributed at the periphery of the structures (Figure 4*D*).

Another property of stemlike cells is their relative resistance to drug treatment. We tested the response of cells to rapamycin treatment and observed that whereas approximately 40% of parental cells underwent apoptosis, Core cells had only 2.6% apoptotic cells and virtually no apoptosis occurred in rapamycin-treated Inv samples (Figures 4*E* and W3, *A* and *B*). Rapamycin inhibits the mammalian target of rapamycin complex 1 (mTORC1), and we confirmed that it effectively suppressed the phosphorylation of $p70^{S6K}$, a downstream mTORC1 target (Figure W3*C*). Paradoxically, it increased Akt-Ser473 phosphorylation in all three populations, most likely by release of an mTORC1-inhibitory feedback loop on PI3K/Akt signaling [20]. It seems that, overall, Inv cells showed a more pronounced phenotype consistent with stem cell behavior than Core cells, explaining most likely the increased oncogenicity of Inv cells *in vivo*.

Opposite Activation of Erk and PI3K/Akt Pathways in Invasive Versus Noninvasive GBM Cells

To address the mechanism of the observed phenotypes in Inv and Core cells, we investigated a series of pathways and molecules involved in proliferation and invasion. Of these, Erk activation was systematically

altered in three distinct pairs of Inv/Core cells (Figure 5*A*). Erk phosphorylation (activation) was upregulated in Core cells and downregulated in Inv cells compared with parental cells (Figure 5*A*), and these differences correlated well with the higher or lower *in vitro* proliferation rates of Core and Inv cells, respectively. To exclude the potentially confounding effects of cell culture, we also performed IHC with phospho-Erk antibody on tumor tissue sections from mice injected with Inv or Core cells. A striking difference not only in phospho-Erk expression but also in subcellular localization was apparent: Core-derived tumors presented very high levels especially in the nuclei of tumor cells, whereas Inv-derived tumors had low cytoplasmic levels. The high nuclear expression of phospho-Erk in Core

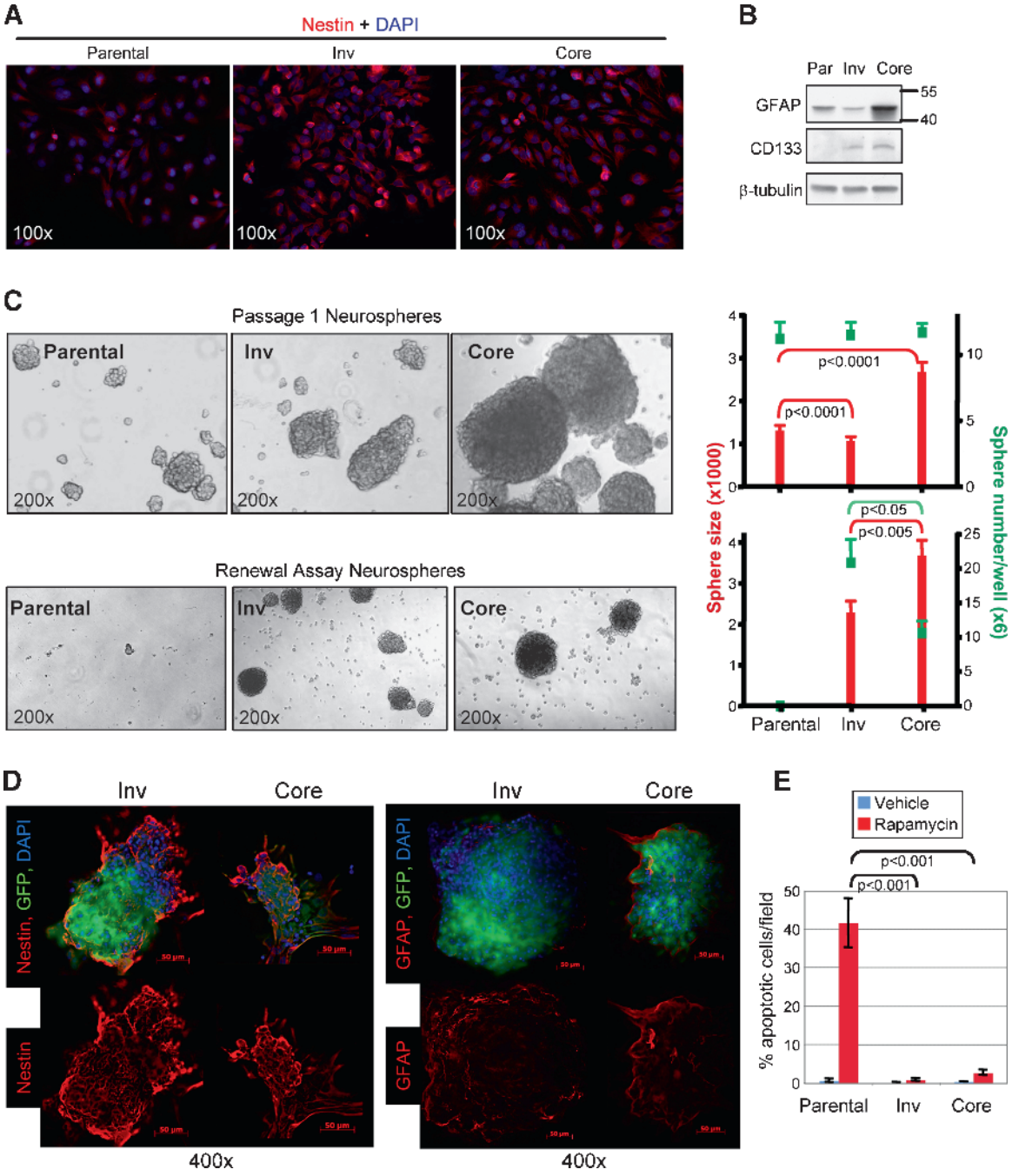

Figure 4. Invasive cells show stem cell characteristics. (A) Immunofluorescence with nestin antibody shows increased staining in Inv cells. (B) Immunoblot analysis with indicated antibodies of protein extracts from U251-MG parental (Par), Inv, and Core cells shows increased GFAP expression in Core cells and gain of CD133 expression in both subpopulations. (C) Bright field images (original magnification, ×200) of passage 1 (upper row) and renewal (lower row) parental, Inv, and Core cell neurospheres. The graphs show the number of spheres in green squares and the sphere size in red bars. Data are means ± SEM from counts of 10 wells. These experiments were repeated three times with similar results. (D) Immunofluorescence with indicated antibodies of Inv and Core renewal neurospheres. Note increased expression of GFAP in Core neurospheres and of nestin in Inv neurospheres. (E) TUNEL apoptosis assay of rapamycin-treated parental, Inv, and Core cells. Data are means ± SEM from quadruplicates. These experiments were repeated three times with similar results.

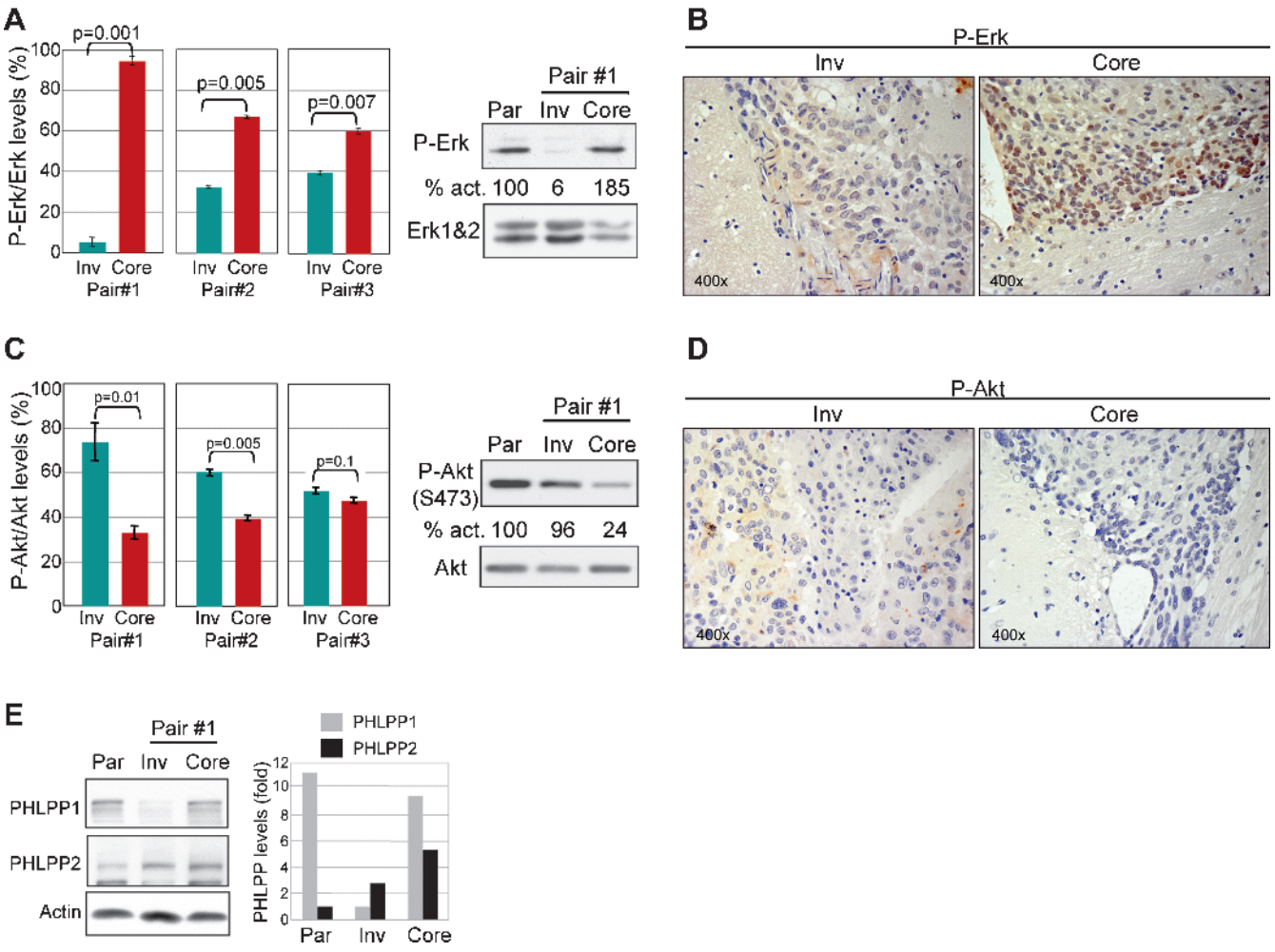

Figure 5. Erk and Akt are differentially activated in Inv *versus* Core cells. (A) Western blot analysis of phosphorylated P-Erk in three pairs of Core and Inv cells derived from three mice (Figure 1*A*). P-Erk levels were normalized to total Erk1 (P-Erk/Erk), and results were represented as means ± SEM from two experiments. The panels show results from Pair #1 compared to parental (Par) cells. The percentage P-Erk/Erk activation (act.) is indicated under the corresponding bands. (B) IHC with P-Erk antibody of tumor sections from mice injected with Inv and Core cells showing high nuclear P-Erk levels in Core tumor cells. (C) Western blot with P-Akt (Ser473) antibody and analysis of P-Akt/Akt activation in the three sets of Inv/Core cells as in panel A. (D) IHC with P-Akt antibody of Inv and Core tumor tissue sections showing higher P-Akt cytoplasmic levels in Inv tumor cells. (E) PHLPP1 and PHLPP2 levels in parental, Inv, and Core cells. The graph represents PHLPP1 and PHLPP2 levels normalized to actin.

tumors strongly suggested that Erk might drive the high proliferation of Core cells leading to the development of bulky tumors in these mice.

Conversely, Akt phosphorylation on Ser473 that reflects its activation was higher in Inv cells than in Core cells, with statistically significant differences in two Inv/Core cell pairs (Figure 5*C*). In this case, the activation of the PI3K/Akt pathway appears important for the higher invasiveness, stemness, and *in vivo* tumorigenicity of Inv *versus* Core cells. IHC of tumor tissue sections with phospho-Akt Ser473 antibody showed a moderate cytoplasmic expression in cells from Inv-derived tumors and absent staining in Core-derived tumors (Figure 5*D*). Overall, phospho-Akt was increased in Inv cells *versus* Core cells but seemed to have similar levels in Inv and parental U251 cells (Figure 5*C*). The major suppressor of the PI3K/Akt pathway is the PTEN tumor suppressor [21]. In U251 cells, PTEN is inactivated by mutation [22], was absent in all three cell populations (not shown), and, therefore, is not a candidate for the observed Akt changes. Recently, PHLPP1 and PHLPP2 have been shown to specifically dephosphorylate Akt phospho-Ser473 and suppress Akt activity [23,24]. Examination of the expression levels of PHLPP1 and PHLPP2 in parental, Inv, and Core cells showed a drop of PHLPP1 in Inv cells, which could explain the increase of phosphorylated Akt in these cells in comparison to Core cells (Figure 5*E*). The levels of PHLPP2 correlated with the levels of phospho-Akt in the three populations, the lowest being in parental cells and the highest in Core cells (Figure 5*E*, *graph*). Overall, Core cells had high levels of both PHLPP1 and PHLPP2, most likely responsible for the very low levels of phospho-Akt in these cells.

Discussion

GBM is a rapidly lethal condition because of the existence of dispersed tumor cells at distant sites within the brain at the time of the surgical resection of the primary tumor. We aimed to reproduce the human condition and characterize the infiltrative GBM cells. We therefore inoculated intracranially a cohort of immunodeficient mice with human GBM cells of low tumorigenic potential to allow for dispersal of the tumor cells before the mice die due to the mass effect of the primary

tumor. Interestingly, during the 3- to 9-month survival interval, two tumor pathologies developed, one with cells resembling parental U251 cells and one with giant multinucleated cells. The latter appeared only in mice surviving more than 5 months after injection and closely resembled the giant cell GBM subtype in humans that, despite its highly atypical histological appearance, has better prognosis [25]. This is the first report of a xenograft model of this tumor subtype, and a relatively benign proliferation and migration phenotype correlating with the phospho-Erk and phospho-Akt levels, respectively, was confirmed in these cells (Figure W4).

We studied more in detail the dispersal of GBM cells in the brain of mice with tumors of parental cell morphology that, in general, developed more rapidly than the giant cell tumors. Isolation of primary tumor Core cells and of invasive Inv cells allowed matched comparison of cells grown *in vivo* in the same conditions. Surprisingly, Inv cells showed a significantly more aggressive phenotype than Core cells when reimplanted in mouse brains, suggestive of the aggressiveness of GBM recurrences in patients. These findings are different from previous studies with human xenografted GBM cells showing an increase in tumorigenicity with decreasing invasive potential of the xenografts [26,27]. However, the difference may come from the different strategies used for obtaining the human GBM xenograft model. Whereas we compared matched Core and Inv cell populations derived from the same animal, these studies compared tumor core cells derived from early animal passages with those from late passages. In our case, both groups of *in vivo*–selected cells were strongly tumorigenic, and no further increase in tumorigenicity was observed on two additional rounds of intracranial inoculations of Inv cells (not shown). This showed that during the first passage in the mouse brain, the initial low-oncogenic parental GBM cells acquired their full tumorigenic potential.

After examining several phenotypical properties, we concluded that the main characteristic that differentiated the *in vivo*–selected cell populations from parental cells was the acquired stemness by *in vivo* growth (Figure 6). In particular, the *in vivo*–selected cells could be propagated as neurospheres, whereas parental cells could not, most likely because of anoikis. More importantly, the *in vivo*–selected cells also became resistant to the apoptotic death that was induced in parental cells by rapamycin treatment. These features that define stem cells [28] were obviously acquired by parental cells during *in vivo* growth but not during the growth within the first-passage neurospheres, implicating the brain microenvironment as responsible for promoting and maintaining these cells in a stem cell–like state [29]. We believe that the parental U251 cells contain a mixture of cells with different properties, including a subpopulation of stemlike cells. This assumption is supported not only by a recent study reporting that U251 cells have a higher percentage of CD133 and nestin-positive cells than other GBM cell lines [30] but also by our *in vitro* cell cloning experiments that identified cell clones with higher or lower Akt activation (not shown). Another argument supporting the existence of different cell subsets in the initial cell population is the development of slowly growing giant cell tumors in half of the injected mice, most likely deriving from a subset of slowly growing cells present in the parental population. A parallel could be drawn between the

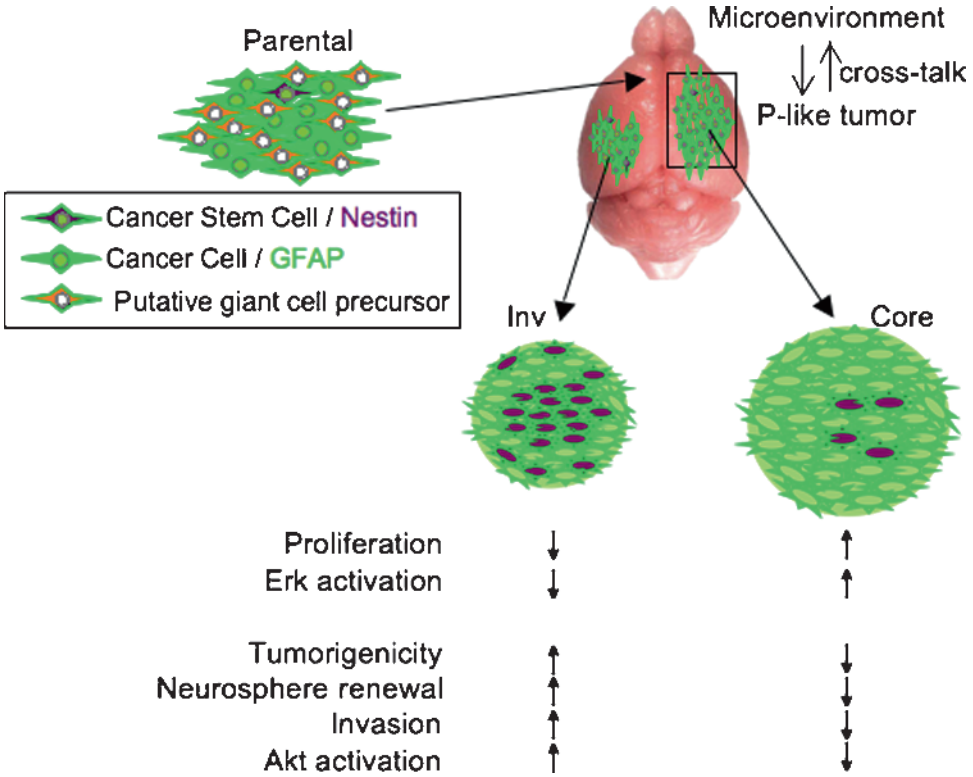

Figure 6. Model of GBM cell invasion. The initial parental population is most likely a mixture of different cell subsets, including putative giant cell precursors giving rise to the giant cell tumors from Figure 1. The cells giving rise to the parental-like (P-like) tumors interact with the brain microenvironment that enriches their stem cell–like state. The resulting Core and Inv cells may also contain different proportions of two cell types: cancer stem cells (expressing nestin) and cancer cells (expressing GFAP). These different proportions would confer the Inv and Core cells their phenotype and signaling signatures.

growth of tumor variants from an initial mixed cell pool and the infection of the host with a mixture of microorganisms. In our studies with mixed viral poliovirus strains of different neuropathogenicities, individual mice were affected randomly by the virus variants from the mixture [31], suggesting an initial stochastic selection in the brain. In the case of tumor cells, the different cell subsets injected would interact with the brain microenvironment and differentiate into different output populations (Figure 6). These output populations may be very obviously different from the parental population, as in the case of the giant cells or, more similar to this, as in the case of the Inv and Core cells. The fact that the brain microenvironment can select populations more and more adapted to it has been previously shown [26,27,32]. These differences may be gradually lost once the cells are removed from the metabolic environment of the brain and placed in traditional cell culture media. Therefore, the migratory phenotype in which we are interested would be partly predetermined, resulting most likely from two processes: a certain preexistent affinity of a cell subpopulation for the ECM and a cross talk between these prespecialized cells and the brain microenvironment.

Increased invasiveness was recently correlated to stem cell properties in various types of cells, including GBM cells that generate invasive tumors [33]. We also observed that Inv cells have a more pronounced stem cell appearance than Core cells, manifested by higher nestin expression, self-renewal ability, and drug-induced resistance to apoptosis. In our case, these characteristics directly correlated with increased *in vivo* and *in vitro* invasiveness. The higher *in vivo* tumorigenicity of Inv cells *versus* Core cells contrasted with their *in vitro* proliferation rate either in the two-dimensional culture or in the three-dimensional neurospheres. However, this finding is in agreement with a previous study with *in vitro*–selected invasive GBM cells in which proliferation markers were downregulated [34] and with the notion that cells with stemlike characteristics have a lower proliferation rate than transit-amplifying cells [35]. It seems that the Inv cells behave as cancer cells with stemlike characteristics, in that they proliferate less, but once established at secondary sites, they upregulate their self-renewal and regrow tumors.

In a large screen with phosphoantibodies, we found that Erk is significantly suppressed in Inv cells and activated in Core cells. In contrast, Akt was activated in Inv cells and inhibited in Core cells. Both of these pathways have been implicated in cell invasion, proliferation, and differentiation, and the PI3K/Akt pathway has also been firmly implicated in the maintenance and self-renewal of pluripotent embryonic stem cells [36]. Whereas it is known that cytokines, growth factors, and ECM components stimulate both pathways simultaneously, an inhibitory cross talk between the PI3K/Akt and Raf/MEK/Erk pathways has been characterized, and it relies on the suppression of Raf kinase activity through phosphorylation of a conserved residue in the regulatory domain by Akt [37]. Interestingly, this inhibition is triggered only by a strong stimulation of the PI3K/Akt pathway and not by stimuli that preferentially activate the Erk pathway [38]. It is important to note that the PI3K/Akt pathway in U251 parental cells is already strongly activated by PTEN deficiency [39] and that PTEN loss of heterozygosity is a frequent event in GBM [1]. It is thus tempting to speculate that the tuning of the PI3K/Akt pathway, most likely by local growth factors and ECM components from the brain microenvironment, regulates in turn the Erk pathway and the ability to invade or proliferate of the GBM cells. In the case of the U251 xenograft, even if all the cells had PTEN deletion, a process of selective spatial positioning most likely took place. Consistent with our model discussed previously, the cells with lower Akt and higher Erk activation underwent selection toward enhanced proliferation in the core of the tumor, and the cells with high Akt and low Erk activation actively invaded the surrounding parenchyma along blood vessels and white matter tracts.

We identified that the activation of Akt was controlled *in vivo* by the PHLPP phosphatases in the U251 PTEN-negative cells. In parental cells, the levels of PHLPP1 were relatively high, whereas those of PHLPP2 were low. In the *in vivo*–selected cells, a switch of the levels took place. Thus, in Inv cells, PHLPP1 was considerably reduced, and its low levels were maintained in invasive cells harvested from mice after two *in vivo* passages of Inv cells (not shown). Conversely, in Core cells, PHLPP2 was increased, resulting in Akt suppression. We have recently shown that PTEN and PHLPP1 depletion synergistically activate Akt in PTEN-positive GBM cells and that the levels of both PHLPP1 and PHLPP2 inversely correlate with Akt activation in PTEN-negative GBM cells (unpublished data). Here, we found that the cells selected their PHLPP levels *in vivo* to adapt the intensity of Akt activation to a proliferative or invasive phenotype.

In summary, we developed in this study a mouse orthotopic model of human invasive GBM. The invasive cells presented stem cell characteristics and increased tumorigenicity. We found high Akt and low Erk activation in the invasive cells and a reversed pattern in the tumor core cells. Because the GBM recurrences in patients arise from invasive cells not removed by the initial surgical resection, these findings prompt consideration of anti-PI3K/Akt inhibitors to target the remaining invasive cells. If an inhibitory Akt-Erk cross talk is present in invasive cells, an unwanted activation of the Erk pathway may ensue from the PI3K/Akt inhibition, resulting in increased local proliferation and recurrence. Therefore, future studies in our model will address these drug escape mechanisms and test combination therapies with inhibitors for both pathways.

Acknowledgments

The authors thank T.J. Liu and Gilbert Cote for valuable advice; Tom Killian, Robert Raphael, and Ramsey Kamar for help with microscopy; and Eliseo Castillo for preparing the NHA-mCherry cells.

References

[1] Ohgaki H and Kleihues P (2007). Genetic pathways to primary and secondary glioblastoma. *Am J Pathol* **170**, 1445–1453.

[2] Hadjipanayis CG and Van Meir EG (2009). Tumor initiating cells in malignant gliomas: biology and implications for therapy. *J Mol Med* **87**, 363–374.

[3] Furnari FB, Fenton T, Bachoo RM, Mukasa A, Stommel JM, Stegh A, Hahn WC, Ligon KL, Louis DN, Brennan C, et al. (2007). Malignant astrocytic glioma: genetics, biology, and paths to treatment. *Genes Dev* **21**, 2683–2710.

[4] McGillicuddy LT, Fromm JA, Hollstein PE, Kubek S, Beroukhim R, De Raedt T, Johnson BW, Williams SM, Nghiemphu P, Liau LM, et al. (2009). Proteasomal and genetic inactivation of the NF1 tumor suppressor in gliomagenesis. *Cancer Cell* **16**, 44–54.

[5] Park JB, Kwak HJ, and Lee SH (2008). Role of hyaluronan in glioma invasion. *Cell Adh Migr* **2**, 202–207.

[6] Knott JC, Mahesparan R, Garcia-Cabrera I, Bolge Tysnes B, Edvardsen K, Ness GO, Mork S, Lund-Johansen M, and Bjerkvig R (1998). Stimulation of extracellular matrix components in the normal brain by invading glioma cells. *Int J Cancer* **75**, 864–872.

[7] Pedersen PH, Marienhagen K, Mork S, and Bjerkvig R (1993). Migratory pattern of fetal rat brain cells and human glioma cells in the adult rat brain. *Cancer Res* **53**, 5158–5165.

[8] Georgescu MM, Kirsch KH, Akagi T, Shishido T, and Hanafusa H (1999). The tumor-suppressor activity of PTEN is regulated by its carboxyl-terminal region. *Proc Natl Acad Sci USA* **96**, 10182–10187.

[9] Lal S, Lacroix M, Tofilon P, Fuller GN, Sawaya R, and Lang FF (2000). An implantable guide-screw system for brain tumor studies in small animals. *J Neurosurg* **92**, 326–333.

[10] Morales FC, Molina JR, Hayashi Y, and Georgescu MM (2010). Overexpresssion of ezrin inactivates NF2 tumor suppressor in glioblastoma. *Neuro Oncol,* E-pub ahead of print Feb 14.

[11] Morales FC, Takahashi Y, Kreimann EL, and Georgescu M-M (2004). Ezrin-radixin-moesin (ERM)–binding phosphoprotein 50 organizes ERM proteins at the apical membrane of polarized epithelia. *Proc Natl Acad Sci USA* **101**, 17705–17710.

[12] Takahashi Y, Morales FC, Kreimann EL, and Georgescu MM (2006). PTEN tumor suppressor associates with NHERF proteins to attenuate PDGF receptor signaling. *EMBO J* **25**, 910–920.

[13] Souza GR, Molina JR, Raphael RM, Ozawa MG, Stark DJ, Levin CS, Bronk LF, Ananta JS, Mandelin J, Georgescu MM, et al. (2010). Three-dimensional tissue culture based on magnetic cell levitation. *Nat Nanotechnol* **5**, 291–296.

[14] Souza GR, Yonel-Gumruk E, Fan D, Easley J, Rangel R, Guzman-Rojas L, Miller JH, Arap W, and Pasqualini R (2008). Bottom-up assembly of hydrogels from bacteriophage and Au nanoparticles: the effect of *cis*- and *trans*-acting factors. *PLoS ONE* **3**, e2242.

[15] Georgescu MM, Kirsch KH, Shishido T, Zong C, and Hanafusa H (1999). Biological effects of c-Mer receptor tyrosine kinase in hematopoietic cells depend on the Grb2 binding site in the receptor and the activation of NF-κB. *Mol Cell Biol* **19**, 1171–1181.

[16] Radaelli E, Ceruti R, Patton V, Russo M, Degrassi A, Croci V, Caprera F, Stortini G, Scanziani E, Pesenti E, et al. (2009). Immunohistopathological and neuroimaging characterization of murine orthotopic xenograft models of glioblastoma multiforme recapitulating the most salient features of human disease. *Histol Histopathol* **24**, 879–891.

[17] Bellail AC, Hunter SB, Brat DJ, Tan C, and Van Meir EG (2004). Microregional extracellular matrix heterogeneity in brain modulates glioma cell invasion. *Int J Biochem Cell Biol* **36**, 1046–1069.

[18] Giese A and Westphal M (1996). Glioma invasion in the central nervous system. *Neurosurgery* **39**, 235–250, discussion 250–232.

[19] Lee J, Kotliarova S, Kotliarov Y, Li A, Su Q, Donin NM, Pastorino S, Purow BW, Christopher N, Zhang W, et al. (2006). Tumor stem cells derived from glioblastomas cultured in bFGF and EGF more closely mirror the phenotype and genotype of primary tumors than do serum-cultured cell lines. *Cancer Cell* **9**, 391–403.

[20] Harrington LS, Findlay GM, and Lamb RF (2005). Restraining PI3K: mTOR signalling goes back to the membrane. *Trends Biochem Sci* **30**, 35–42.

[21] Sulis ML and Parsons R (2003). PTEN: from pathology to biology. *Trends Cell Biol* **13**, 478–483.

[22] Steck PA, Pershouse MA, Jasser SA, Yung WK, Lin H, Ligon AH, Langford LA, Baumgard ML, Hattier T, Davis T, et al. (1997). Identification of a candidate tumour suppressor gene, *MMAC1*, at chromosome 10q23.3 that is mutated in multiple advanced cancers. *Nat Genet* **15**, 356–362.

[23] Brognard J, Sierecki E, Gao T, and Newton AC (2007). PHLPP and a second isoform, PHLPP2, differentially attenuate the amplitude of Akt signaling by regulating distinct Akt isoforms. *Mol Cell* **25**, 917–931.

[24] Gao T, Furnari F, and Newton AC (2005). PHLPP: a phosphatase that directly dephosphorylates Akt, promotes apoptosis, and suppresses tumor growth. *Mol Cell* **18**, 13–24.

[25] McLendon RE, Friedman AH, and Gray L (2006). *Glioblastoma* (7th ed). Hodder Arnold, London, UK.

[26] Johannessen TC, Wang J, Skaftnesmo KO, Sakariassen PO, Enger PO, Petersen K, Oyan AM, Kalland KH, Bjerkvig R, and Tysnes BB (2009). Highly infiltrative brain tumours show reduced chemosensitivity associated with a stem cell–like phenotype. *Neuropathol Appl Neurobiol* **35**, 380–393.

[27] Sakariassen PO, Prestegarden L, Wang J, Skaftnesmo KO, Mahesparan R, Molthoff C, Sminia P, Sundlisaeter E, Misra A, Tysnes BB, et al. (2006). Angiogenesis-independent tumor growth mediated by stem-like cancer cells. *Proc Natl Acad Sci USA* **103**, 16466–16471.

[28] Reya T, Morrison SJ, Clarke MF, and Weissman IL (2001). Stem cells, cancer, and cancer stem cells. *Nature* **414**, 105–111.

[29] Calabrese C, Poppleton H, Kocak M, Hogg TL, Fuller C, Hamner B, Oh EY, Gaber MW, Finklestein D, Allen M, et al. (2007). A perivascular niche for brain tumor stem cells. *Cancer Cell* **11**, 69–82.

[30] Qiang L, Yang Y, Ma YJ, Chen FH, Zhang LB, Liu W, Qi Q, Lu N, Tao L, Wang XT, et al. (2009). Isolation and characterization of cancer stem like cells in human glioblastoma cell lines. *Cancer Lett* **279**, 13–21.

[31] Georgescu MM, Balanant J, Ozden S, and Crainic R (1997). Random selection: a model for poliovirus infection of the central nervous system. *J Gen Virol* **78**, 1819–1828.

[32] Hoelzinger DB, Demuth T, and Berens ME (2007). Autocrine factors that sustain glioma invasion and paracrine biology in the brain microenvironment. *J Natl Cancer Inst* **99**, 1583–1593.

[33] Wakimoto H, Kesari S, Farrell CJ, Curry WT Jr, Zaupa C, Aghi M, Kuroda T, Stemmer-Rachamimov A, Shah K, Liu TC, et al. (2009). Human glioblastoma-derived cancer stem cells: establishment of invasive glioma models and treatment with oncolytic herpes simplex virus vectors. *Cancer Res* **69**, 3472–3481.

[34] Mariani L, Beaudry C, McDonough WS, Hoelzinger DB, Demuth T, Ross KR, Berens T, Coons SW, Watts G, Trent JM, et al. (2001). Glioma cell motility is associated with reduced transcription of proapoptotic and proliferation genes: a cDNA microarray analysis. *J Neurooncol* **53**, 161–176.

[35] van der Flier LG and Clevers H (2009). Stem cells, self-renewal, and differentiation in the intestinal epithelium. *Annu Rev Physiol* **71**, 241–260.

[36] Dreesen O and Brivanlou AH (2007). Signaling pathways in cancer and embryonic stem cells. *Stem Cell Rev* **3**, 7–17.

[37] Zimmermann S and Moelling K (1999). Phosphorylation and regulation of Raf by Akt (protein kinase B). *Science* **286**, 1741–1744.

[38] Moelling K, Schad K, Bosse M, Zimmermann S, and Schweneker M (2002). Regulation of Raf-Akt cross-talk. *J Biol Chem* **277**, 31099–31106.

[39] Radu A, Neubauer V, Akagi T, Hanafusa H, and Georgescu MM (2003). PTEN induces cell cycle arrest by decreasing the level and nuclear localization of cyclin D1. *Mol Cell Biol* **23**, 6139–6149.

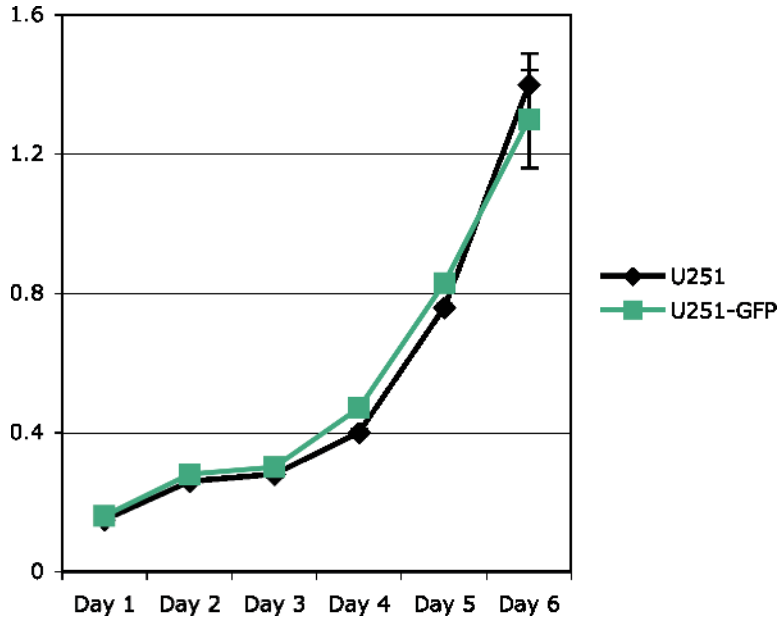

Figure W1. MTT proliferation assay of U251-MG cells either noninfected (U251) or infected with retroviruses carrying pCX_p-GFP vector for stable GFP expression (U251-GFP). Note no difference in proliferation induced by GFP expression.

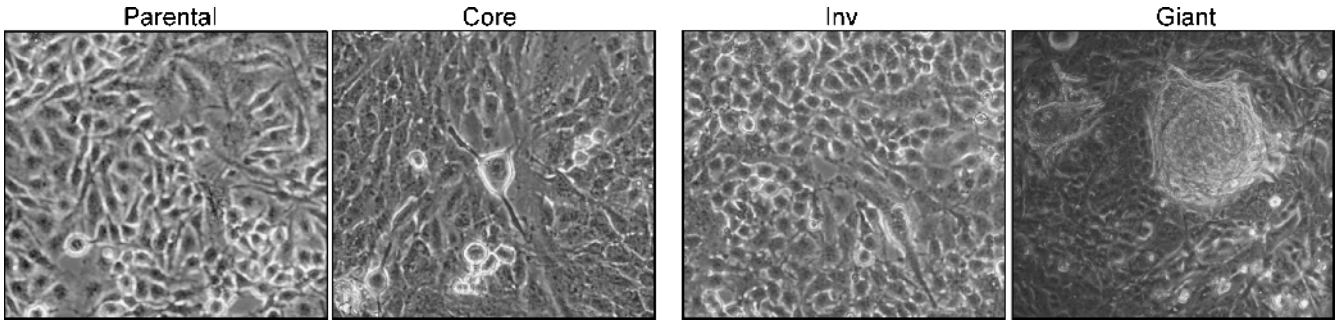

Figure W2. Morphology of parental U251-MG cells and of the cells isolated from the animals 1 (Core and Inv) and 9 (giant) from Figure 1*A*. Bright field images at an original magnification of ×400.

Figure W3. Resistance to apoptosis induced by rapamycin treatment of *in vivo*–selected Inv and Core cells. (A) Control TMR Red apoptosis assay showing 100% apoptosis by treatment with DNase I of parental U251-MG cells labeled with GFP. Apoptosis was recognized by treating the fixed permeabilized cells with terminal deoxynucleotidyl transferase followed by treatment with TMR Red to label the DNA strand breaks. Double-labeled nuclei appear yellow in the merged image. (B) Parental, Inv, and Core cells were treated with 100 nM rapamycin for 72 hours and assayed for apoptosis. Four images were recorded per chamber in both green and red channels with a Zeiss Axiovert 200M inverted microscope, and the number of red cells (apoptotic) was calculated from the total number of cells (green cells; graph in Figure 4*D*). (C) Parental, Inv, and Core cells were treated with the indicated doses of rapamycin for 72 hours. Cells were lysed and analyzed by immunoblot analysis with antibodies for P-$p70^{S6K}$, a downstream target of mTORC1, and P-Akt (Ser473), target of mTORC2. Note efficient inhibition of $p70^{S6K}$ phosphorylation by rapamycin treatment. In contrast, Akt phosphorylation was increased in the same conditions. Note also higher basal Akt phosphorylation of Inv cells compared with Core cells.

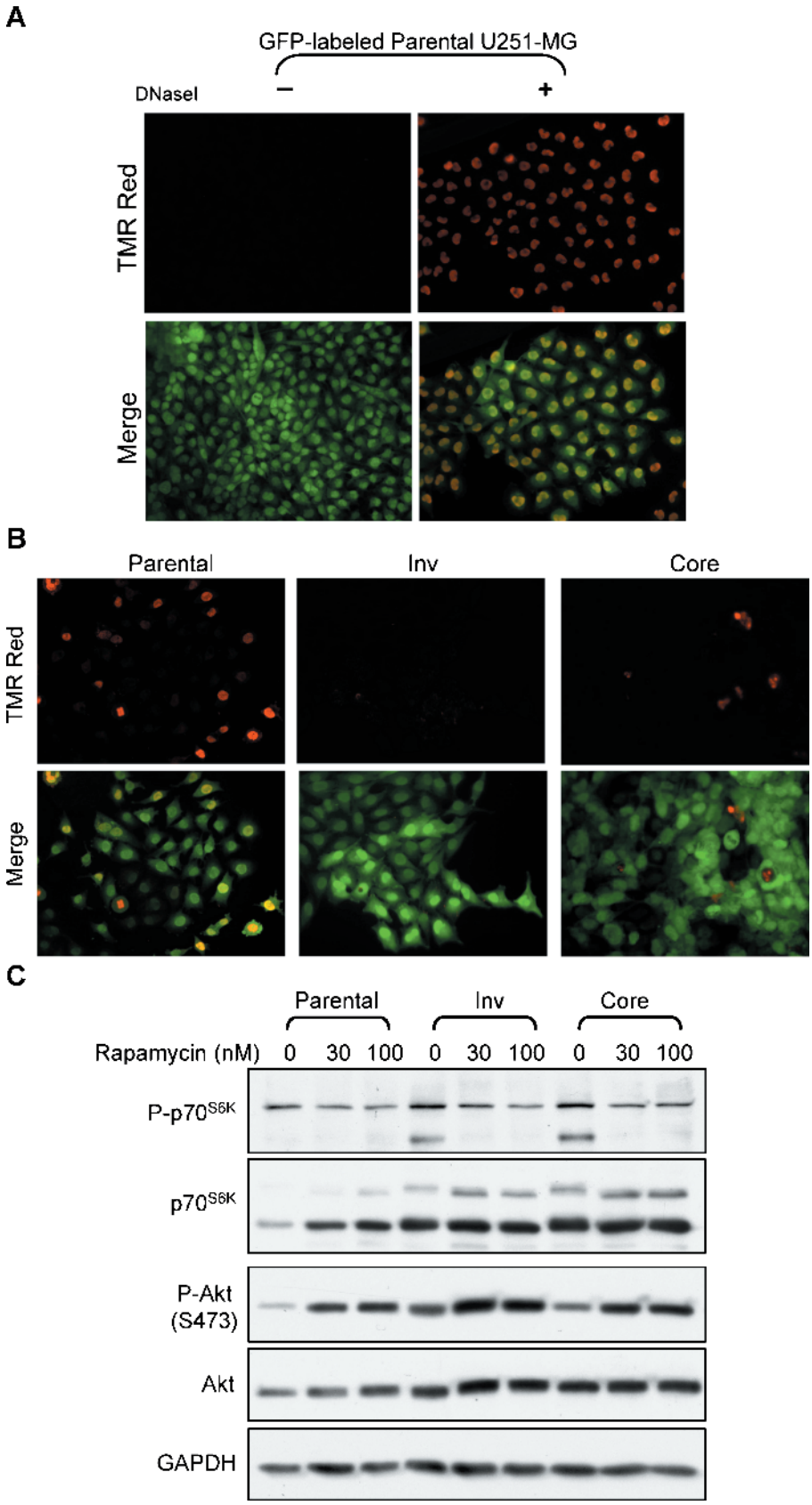
A
GFP-labeled Parental U251-MG
DNaseI
–
+
TMR Red
Merge
B
Parental
Inv
Core
TMR Red
Merge
C
Parental
Inv
Core
Rapamycin (nM) 0 30 100 0 30 100 0 30 100
P-p70S6K
p70S6K
P-Akt (S473)
Akt
GAPDH

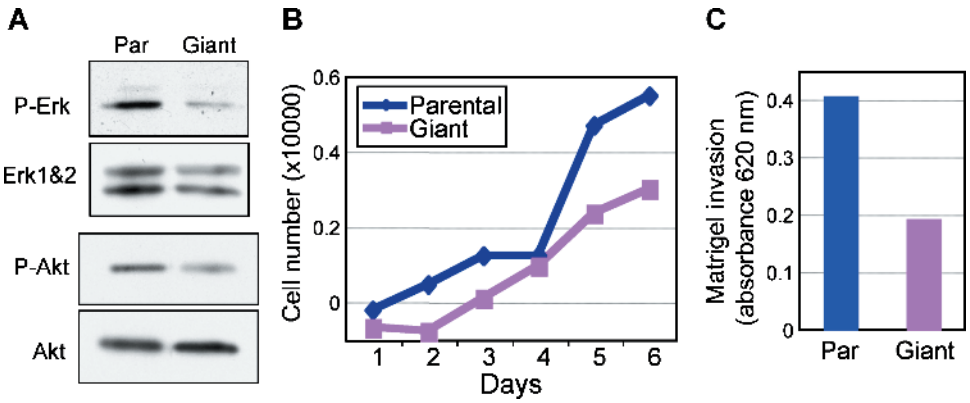

Figure W4. Reduced signaling, proliferation, and invasion of giant cells in comparison to parental U251 cells. (A) Western blot analysis of protein extracts from parental (Par) and giant cells with antibodies against phosphorylated Erk and Akt (S473) and control total Erk1 and 2 and Akt. (B) MTT assay of parental and giant cells showing proliferation during a 6-day period. (C) Matrigel invasion assay showing very reduced invasion of giant cells compared with parental (Par) cells.